2728
doi:10.1017/S1431927621009600
Microsc. Microanal. 27 (Suppl 1), 2021

Phase Evolution Analysis During Real-Time Solid-State Chemical Lithiation of Crystalline Thin Window Silicon Membranes Using Low-Loss STEM-EELS Imaging

Vladimir Oleshko

NIST, Gaithersburg, Maryland, United States

Silicon is one of the most promising anode materials for high-energy-density Li-ion batteries with an exceptional capacity of 3579 mAh g^{-1} assuming $Li_{15}Si_4$ [1, 2]. Its practical use, however, is hindered by high volume expansion (up to 280%) during Li insertion often resulted in contact loss with electrodes and rapid capacity fading. Various advanced designs of nanostructured Si-based composite anodes have been employed to demonstrate their high performance and better accommodate strain while allowing shorter diffusion lengths for Li^+ ions and faster charge/discharge rates. Meanwhile, a fundamental understanding of phase structures, compositions, and transformations during lithiation of Si and kinetic mechanisms is still lacking [3].

Herein, we report an investigation of Li-Si phase evolution under real-time solid-state chemical lithiation of single-crystalline *c*-Si membranes by probe-corrected scanning and transmission electron microscopy (S/TEM) coupled with electron energy-loss spectroscopy (EELS). After Li evaporation on to 35 nm-thick windows < 100 >-oriented *p*-doped Si membranes were safely transferred to a microscope using a vacuum transfer TEM holder. Low-loss EEL spectra of such a membrane are dominated by plasmon peaks, which positions are directly related to valence electron densities n as $E_p = \hbar\omega_p$, $\omega_p=[ne^2/\varepsilon_0 m]^{0.5}$. No metallic Li was detected 30 minutes after Li evaporation indicating fast reactive lithiation kinetics. Using experimental and theoretical data from the Lorentz-Drude model and DFT calculations [1, 3], we have described relationships between $E_p^2 \propto n$ vs. Li content x for various Li-Si intermetallic phases by an exponential decay function, $E_p^2 = A_1\exp(-x/t_1)+y_0$, where least-squares-(*lsq*) fitted parameters A_1=-18.5±8.5, t_1=-38.5±6.1, and y_0=304.8±18.2, respectively (Fig. 1a). Determining phase and chemical compositions and thickness from a Kramers-Kronig sum rule by HAADF STEM-EEL spectroscopic imaging, we have found a Li-rich metastable silicide glass with an atomic ratio of Li/Si » 2.2, close to a Li_7Si_3 that coexists with *c*-Si (Figs. 1b and 2). The Lorentz-Drude models for *c*-Si (Fig. 1b, red curve) and metastable *m*-Li_7Si_3 (Fig. 1b, green curve) were utilized for non-linear least-squares (NLLS) fitting of the spectra for each phase and total fit to derive the local phase distributions. In the absence of an external electric field, room temperature lithiation of *c*-S is driven by the Li concentration gradient and proceeds via Li-consuming fast silicidation reaction which involves diffusive solid-state amorphization (Fig. 2). With an increasing extent of lithiation together with transformations of the electronic band structure, the Si-Si bonds in the diamond *c*-Si structure are successively broken, resulting in the sequential formation of ordered 1 to 2 nm five-membered or four-membered Si clusters distributed in the Si matrix distorted by mechanical stresses. However, room temperature recrystallization of equilibrium intermetallic Li-Si phases appeared frustrated, and after the initial fast reaction step, the metastable silicide glass did not further evolve towards the Li-richest $Li_{15}Si_4$ phase. The obtained results are compared with liquid phase electrochemical lithiation of *c*-Si in a $LiClO_4$-dimethyl carbonate electrolyte when a solid electrolyte interface is present [1] and direct injection of Li^+ ions into *c*-Si using focused Li^+ ion beams [4].

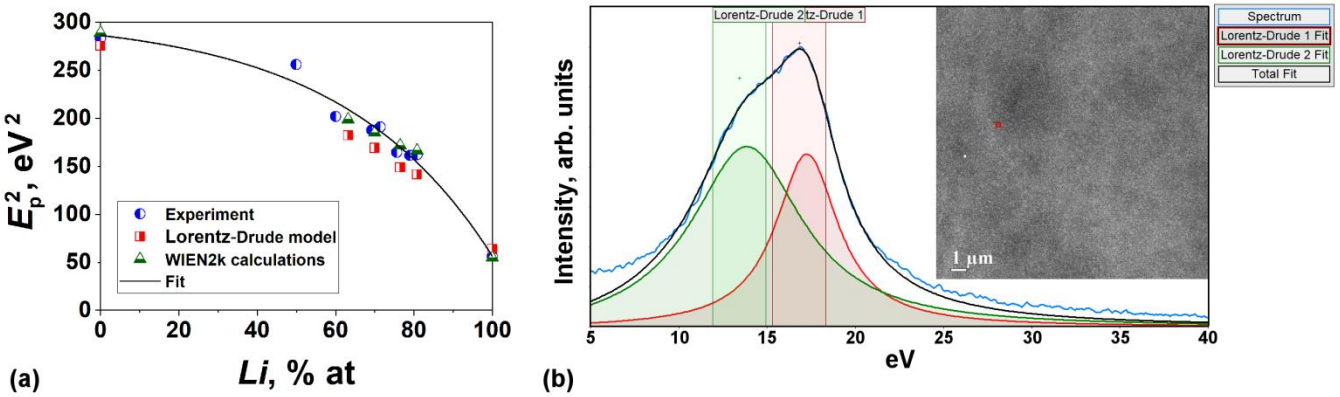

Figure 1. Figure 1. (a) Experimental and calculated values of Ep2 for different Li-Si alloys vs. Li content lsq-fitted with an exponential decay function Ep2 = A1exp(-x/t1)+y0, A1=-18.5±8.5, t1=-38.5±6.1, y0=304.8±18.2. (b) Low-loss EEL spectrum (a single scattering distribution, blue) acquired from the area marked by the red box in (b) shows plasmon peaks at 13.7 eV assigned to a Li7Si3 glass and the bulk Si plasmon at 16.8 eV. Two Lorentz-Drude models (red and green curves) used for NLLS fitting of the spectrum for Li7Si3 and c-Si, respectively, and the total fit (black curve) are shown. HAADF STEM (inset) demonstrates random mass-thickness variations over a lithiated membrane.

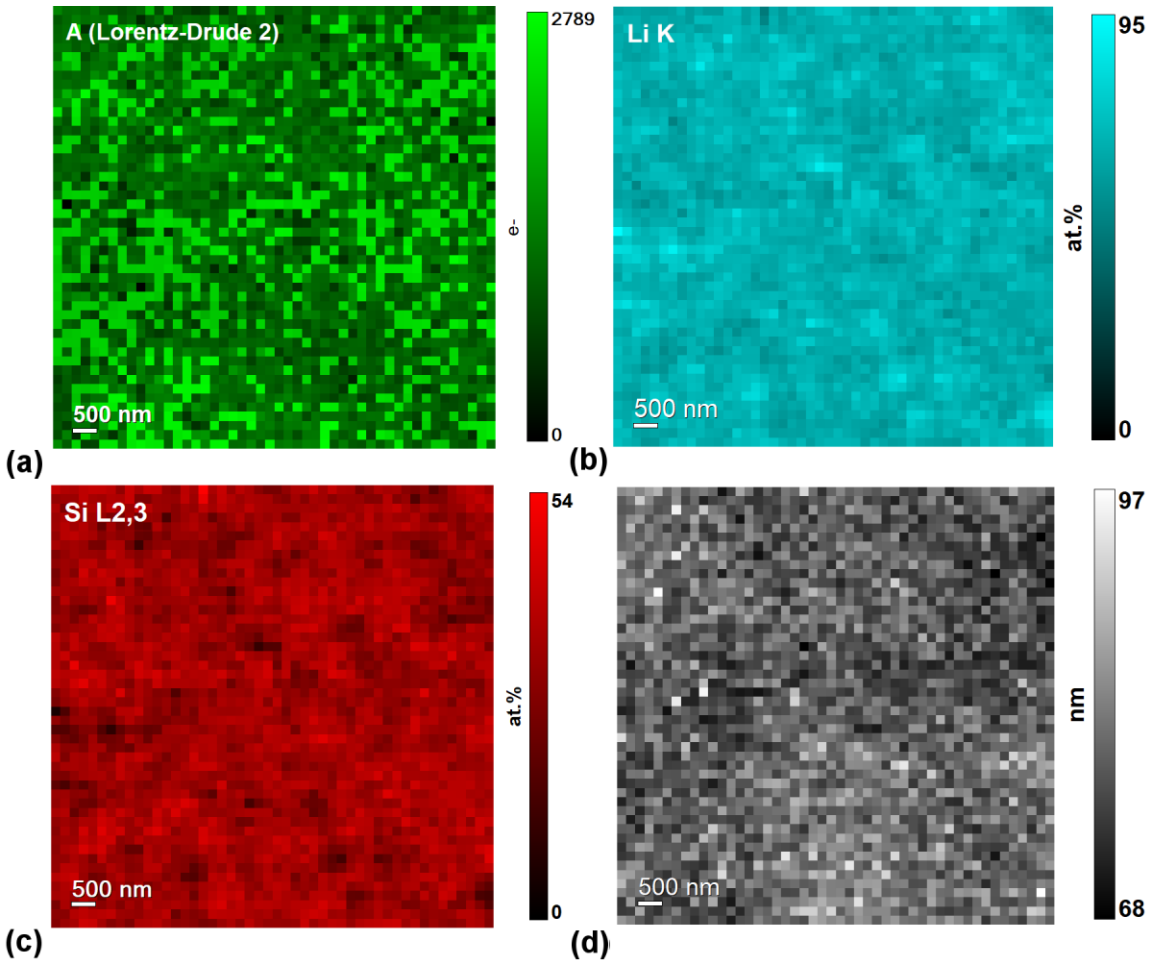

https://doi.org/10.1017/S1431927621009600 Published online by Cambridge University Press

Figure 2. Figure 2. STEM-EELS SI of a lithiated Si window area: (a) Li7Si3 phase distribution derived by NLLS fitting according to a procedure shown in Fig1b; (b) quantitative Li K map; (c) quantitative Si L2,3 map; (d) absolute thickness map derived using a Kramers-Kronig sum rule and refractive index of Si, n =3.98, t/λ varied from 0.3 up to 1.1.

References

[1] VP Oleshko, *et al*, *Microsc. Microanal*. **24** (S1), (2018) 1480; ibid **26** (S2) (2020) 1448.
[2] Choi JW, Aurbach D (2016) *Nature Rev* **1**,1-16.
[3] Boniface, M., *et al* (2016) *Nano Lett.* **16**, 7381-7388.
[4] McGehee W.A., *et al*, *ACS Nano* (2019) **13**, 8012-8022

https://doi.org/10.1017/S1431927621009600 Published online by Cambridge University Press